

RSC Advances

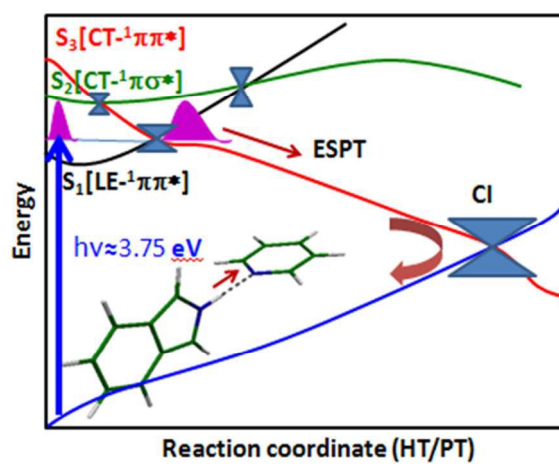


This is an *Accepted Manuscript*, which has been through the Royal Society of Chemistry peer review process and has been accepted for publication.

Accepted Manuscripts are published online shortly after acceptance, before technical editing, formatting and proof reading. Using this free service, authors can make their results available to the community, in citable form, before we publish the edited article. This *Accepted Manuscript* will be replaced by the edited, formatted and paginated article as soon as this is available.

You can find more information about *Accepted Manuscripts* in the [Information for Authors](#).

Please note that technical editing may introduce minor changes to the text and/or graphics, which may alter content. The journal's standard [Terms & Conditions](#) and the [Ethical guidelines](#) still apply. In no event shall the Royal Society of Chemistry be held responsible for any errors or omissions in this *Accepted Manuscript* or any consequences arising from the use of any information it contains.

Graphical Abstract

CC2 potential energy profiles of the ground and excited states of isoindole-pyridine complex along the proton transfer reaction coordinate.

A theoretical exploration on the nonradiative deactivation of hydrogen-bond complexes: isoindole-pyridine and quinoline-pyrrole

Reza Omidyan* Mohammad Salehi and Gholamhassan Azimi

Department of Chemistry, University of Isfahan, 81746-73441 Isfahan, Iran.

Abstract

The second order approximate Moller-plesset (MP2) and Coupled cluster (CC2) methods have been employed to investigate the geometry, electronic transition energies and photophysics of isoindole-pyridine and quinoline-pyrrole complexes. The most stable geometry of both isoindole-pyridine and quinoline-pyrrole complexes, has been predicted to be a perpendicular structure. It has also been found that the first electronic transition in both complexes, is responsible for UV absorption owing to its $^1\pi\pi^*$ nature, while, a charge transfer $^1\pi\pi^*$ state, governs the nonradiative relaxation processes of both complexes. In this regard, the excited state intermolecular hydrogen/proton transfer (ESHT/PT) via the charge transfer electronic states plays the most prominent role on non-radiative deactivation. In the HT/PT reaction coordinate, the minimum potential energy profile of the lowest CT- $^1\pi\pi^*$ state, predissociates the local $^1\pi\pi^*$ state, connecting the latter to a curve crossing with the S_0 state. At the region of this curve crossing, the S_0 and CT state become degenerate, enabling the $^1\pi\pi^*$ state to proceed as predissociative state and finally direct the excited system to the ground state.

1-Introduction

During last two decades, massive attention has been paid to hydrogen bonding in chemistry and biochemistry, because of its fundamental implication and importance in many branches of science^{1, 2}. It has been established that understanding of microscopic structures and functions in many molecular systems, such as hydrogen-bonded water or alcohol networks, organic compounds in solution, hydrogen-bond crystal engineering, polymers, proteins, and DNA^{1, 3-6} are

*Corresponding Author: E-mail: r.omidyan@sci.ui.ac.ir; reza.omidyan@u-psud.fr.
Tell: (+98) 311 7934636. Fax:(+98) 311 6689732.

directly connected to hydrogen bond interactions. In the influential work of Watson and Crick⁷, it has been proposed that the genetic code is stored in the form of hydrogen-bonds between the canonical nucleic acid bases, which form the main frame of DNA molecule. They recognized that tautomerization alters the hydrogen-bonding patterns and therefore could lead to mismatches in the canonical base pairs.

The ground-state properties of hydrogen bonds in molecular systems have been extensively explored by various experimental and theoretical methods^{1, 3, 4, 8-10}. Upon photoexcitation of hydrogen-bonded systems, the hydrogen donor and acceptor molecules reorganize due to the significant difference in the charge distribution of different electronic states¹. The charge rearrangement in excited systems may trigger the photophysical phenomenon of hydrogen/proton transfer, which is called the “Excited State Hydrogen Transfer (ESHT)”. The ESHT is an important subject in the wide range of science, chemistry and biochemistry^{5, 6, 11-13}.

Based on the influential work of Sobolewski and coworkers on pyrrole-pyridine hydrogen bonded dimer¹⁴, it has been remarked that the common feature in photochemistry of hydrogen bonded systems is the electron-driven proton transfer (EDPT) mechanism. Particularly, in these systems, a polar charge transfer state of $^1\pi\pi^*$ nature forces the proton transfer. The HT/PT process may direct the excited system to a conical intersection of the S_1 and S_0 surfaces¹⁴. Later, they¹⁵ demonstrated that potential-energy functions of the lowest locally excited $^1\pi\pi^*$ states of guanine-cytosine complex, are crossed along the proton-transfer reaction path by the reactive potential-energy function of the charge transfer (CT) state. The PE curve crossings evolve to the conical intersections (CIs)¹⁶ in the multidimensional pictures. These CIs influence nonadiabatic processes and facilitate upper state to lower state transitions¹⁶⁻¹⁹. Thus, a barrierless access to the charge transfer (CT)-ground state (S_0) conical intersection, leads the excited system to the electronic ground state, by an ultrafast radiationless decay mechanism. This conclusion indicates the high photostability of guanine-cytosine base pair, against UV radiation as well¹⁵.

Recently, Esboui and Jaidane²⁰ performed a comparative theoretical study on the nonradiative decay mechanisms of the phenol-pyridine complex, a hydrogen bonded cluster. They have predicted that relaxation mechanism involves internal conversion (IC) and intersystem crossing (ISC) along the O-H bond elongation coordinate. Indeed, the excited state proton transfer reaction, mediated by electron transfer, from phenol to pyridine, governs the photophysics of phenol-pyridine complex.

Moreover, based on the previous investigations on the hydrogen-bonded cluster systems, the $^1\pi\pi^*$ excited electronic state has been identified to play the most important photophysical role²¹⁻²⁴, while for the organic compounds, having intramolecular hydrogen bonding, this process is mostly derived by a repulsive $^1\pi\sigma^*$ state^{24, 25}.

In the present study, we focus on the photophysics of two hydrogen-bonded complexes; isoindole-pyridine and quinoline-pyrrole, which are two model-systems, for which the proton donor and acceptor are π -electron conjugated systems. This type complexes can also be considered as a model for fluorescence quenching via intermolecular hydrogen bonding between aromatic chromophores²⁶. Consequently, this work will be helpful for understanding the quenching mechanism of isoindole and quinoline in the excited state by pyridine and pyrrole.

Isoindole, a benzo-fused pyrrole, is an isomer of indole. Isoindole's units occur in phthalocyanines, an important family of dyes. Some alkaloids containing isoindole have been isolated and characterized²⁷. Also, quinoline is homologue of naphthalene, which one of its C-H groups is substituted with nitrogen. These type of compounds are identified as polycyclic aromatic nitrogen heterocycles (PANHs)²⁸, which are interesting from an astrobiological perspective (see Ref. ²⁹ and references there in). Thus, we will present ground- and excited-state optimized structures, transition energies and oscillator strengths of isoindole, quinoline, and also their mixed complexes. Then, we discuss and explain the hydrogen/proton transfer in isoindole-pyridine and quinoline-pyrrole complexes as well.

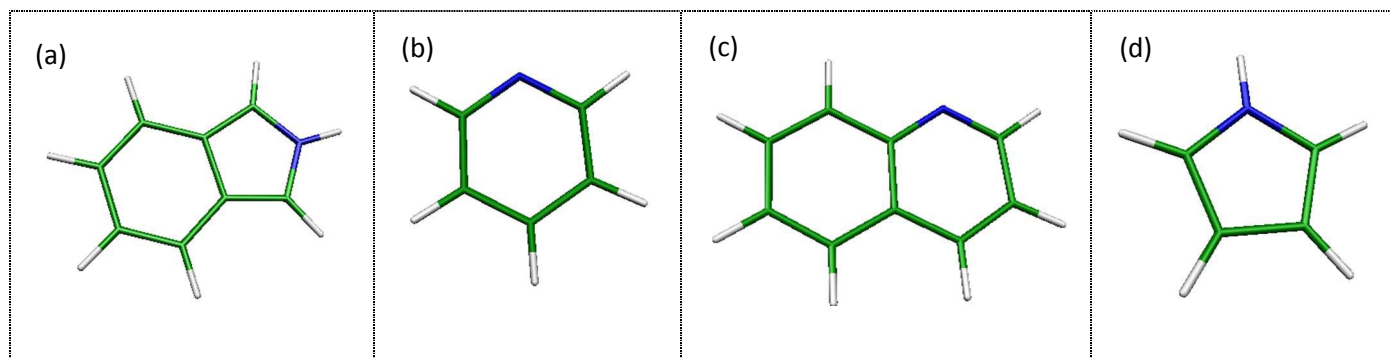


Figure 1. MP2 optimized structure of monomers involved on the structure of complexes, considered in this work: (a) isoindole; (b) pyridine (c) quinoline, (d) pyrrole.

2- Computational details:

The “*ab initio*” calculations have been performed with the TURBOMOLE program suit^{30, 31}, making use of the resolution-of-identity (RI) approximation for the evaluation of the electron repulsion integrals. The equilibrium geometry of all systems at the ground state has been determined at the MP2 (Moller-Plesset second order perturbation theory) level^{32, 33}. Excitation energies and equilibrium geometry of the lowest excited singlet states have been determined at the RI-CC2 (the second-order approximate coupled-cluster method)^{34, 35}. The correlation-consistent polarized valence double-zeta (cc-pVDZ) and the aug-cc-pVDZ³⁶ have been employed for most of calculations. All of the potential energy curves have been determined with the use of aug-cc-pVDZ basis function for all atoms.

The abbreviations of *iIn*, *Q*, *Pl* and *Pn* will be used here after for isoindole, quinoline, pyrrole and pyridine respectively. In addition, the *LE* and *CT* terms will be employed indicating the local excitation and charge transfer transitions respectively. Moreover, in some cases, we will use the “*perp.*” phrase instead of perpendicular word. The pyrrole, pyridine, isoindole monomers and isoindole-pyridine complex have C_{2v} symmetry, while, the quinoline and quinoline-pyrrole complex belong to the C_s symmetry point group. With exception of few calculations (we will address evidently), the symmetry point group of the systems was taken to account for geometry optimization of ground and excited states.

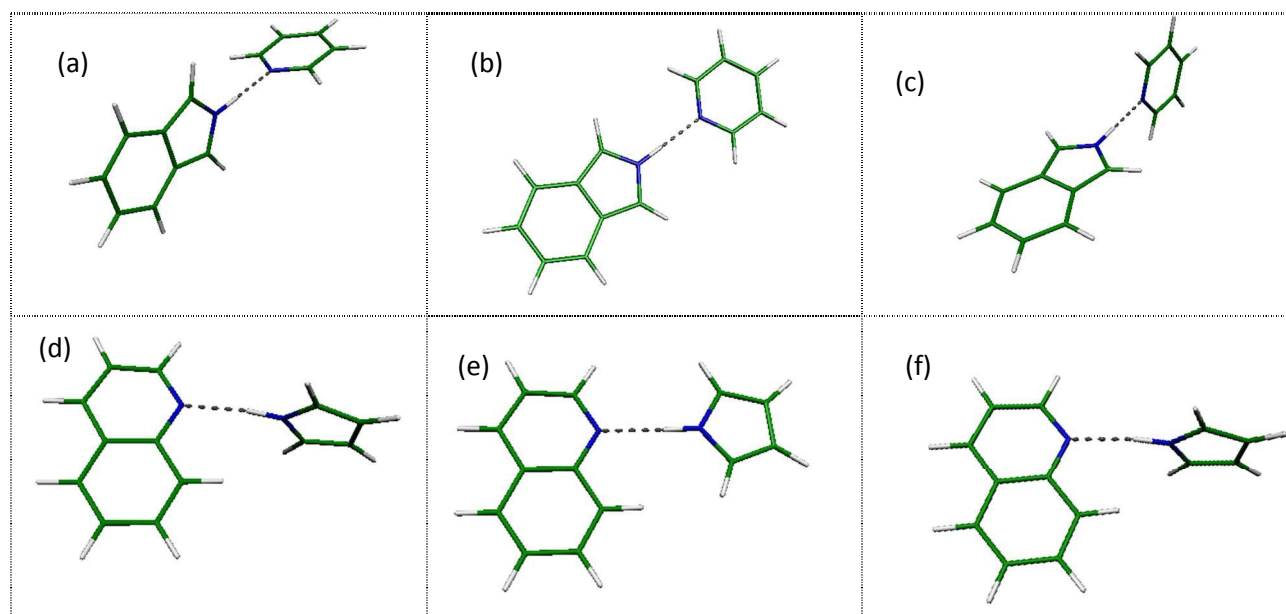


Figure 2. Complex systems considered in this work:

- a) Perpendicular structure of isoindole-pyridine complex (C_{2v} symmetry)
- b) Planar structure of isoindole-pyridine complex (C_s symmetry)
- c) Optimized structure of isoindole-pyridine complex without symmetry constraint.
- d) Perpendicular structure of quinoline-pyrrole complex (C_s symmetry).
- e) Planar structure of quinoline-pyrrole complex (C_s symmetry)
- f) Optimized structure of quinoline-pyrrole complex without symmetry constraint

3- Results and discussion:

3.1. Ground state equilibrium structures and excitation energies of monomers

3-1-a) Pyridine and pyrrole

The electronic and geometry structures of pyridine and pyrrole have been well studied, experimentally and theoretically³⁷⁻⁴⁴. Both systems have been identified as planar structures,^{45,26} having C_{2v} symmetry point group. Excellent summaries from state of knowledge on pyridine can be found in the reviews of Ross⁴⁴, Moomaw⁵² and Zewail⁴³. Pyrrole, also is a prototype of heteroatomic aromatic compound⁴², which has been under intense experimental and theoretical studies^{40, 46}. In particular, the deactivation of photoexcited pyrrole could serve as a model for photodynamical processes of heteroatomic aromatic systems whose $^1\pi\sigma^*$ transition energy is lower than that of the $^1\pi\pi^*$ state. From photophysical aspects, pyrrole and pyridine have been identified as photoacid and photobase systems respectively²⁶. However, we disregard to present further details on physical properties of these two well-known compounds, instead we attend to other monomers; (i.e. isoindole and quinoline), for which less information is found in literature.

3-1-b) Indole, isoindole and quinoline monomers

Indole is the familiar chromophore of tryptophan amino acid and isoindole is its isomer. Indole has been subject of several reports (for instance, see Ref.^{47, 48} and references there in). In contrast, rarely report can be found in literature, dedicated either to electronic structure or physical properties of isoindole. The same story is true about quinoline. Thus, we briefly attend

to geometry and electronic properties of these two monomers. In the full geometry optimization, the MP2 calculated results show that both structures are planar at ground state.

The first electronic transition (${}^1L_b-S_0$) of indole has been investigated experimentally and theoretically. The S_1 (${}^1\pi\pi^*$) band origin of indole has been reported by Mani and Lombardi to 35 232 cm^{-1} (4.37 eV)^{49, 50}. We have determined the adiabatic transition energy of indole at the RI-CC2/aug-cc-pVDZ level amount to 4.57 eV which is comparable with experimental value of Mani and Lombardi with an error of +0.2 eV. Based on the comparative theoretical study of Aquino^{51, 52} this error is normally related to overestimation of CC2 method.

The vertical transition energies for the first two lowest singlet excited states of isoindole have been determined on the basis of ground state optimized geometry. The results have been presented in Table 1.

Based on the C_{2v} symmetry point group, the first electronic transition of isoindole belongs to the B_1 irreducible representation. The S_1-S_0 transition corresponds to single electron transitions of HOMO-LUMO+8 (61%) and HOMO-LUMO+7 (30%). The frontier molecular orbitals of isoindole have been displayed in Figure 3. As shown, the HOMO, LUMO+7 and LUMO+8 orbitals of isoindole have π and π^* nature respectively. Thus its first electronic excited state is of the ${}^1\pi\pi^*$ character. The $1({}^1A_2)$ state corresponds to the second (S_2-S_0) electronic transition of isoindole, arising from HOMO-LUMO single electron transition (83%). As shown in Figure 3, the HOMO is a π , and LUMO is a σ^* orbital which is located over the N-H bond. Hence, the S_2 (1A_2) excited state of isoindole is of the ${}^1\pi\sigma^*$ character. More information about excitation energies, oscillator strengths and their relevant configurations is presented in ESI file.

	Electronic state	Vertical Transition Energy/eV	Oscillator strength	Adiabatic Transition Energy/eV
Isoindole	S ₁ (B ₁)1 [¹ ππ*]	4.15	0.0841	3.91 ^a 3.70
	S ₂ (A ₂)1 [¹ πσ*]	4.21	0.0000	-
Pyridine	S ₁ (B ₂)1 [¹ nπ*]	4.98 ^b 4.98 ^c 4.74	0.0046	4.54 ^b 4.41 ^c 4.31
	S ₂ (B ₁)1 [¹ nσ*]	5.21	0.0310	-
Pyrrole	S ₁ (A ₂)1 [¹ πσ*]	5.02	0.0000	4.81
	S ₅ (B ₁)1 [¹ ππ*]	6.22 ^b 5.85	0.1934	6.00 ^d 5.82
quinoline	S ₁ (A')1 [¹ ππ*]	4.37	0.0247	4.22 ^h 3.99 eV
	S ₂ (A'')1 [¹ σπ*]	4.44	0.0018	

Table 1: Excited transition energies (vertical and adiabatic), of the considered monomers in this work (pyridine, pyrrole, isoindole and quinoline), computed at the CC2/aug-cc-pVDZ level of theory.

a) The experimental value for S₁, 0-0 band of isoindole has been adopted from ref⁵³.

b) The CASPT2 theoretical values for S₁ vertical and adiabatic transition energies of pyridine and pyrrole have been taken from ref.³⁸

c) The corresponding experimental values for S₁ vertical and adiabatic transition energies of pyridine have been adopted from and ref⁵⁴.

d) The experimental value for S₁ 0-0 band of pyrrole has been adopted from ref⁵⁵.

h) The experimental value for S₁ 0-0 band of quinoline has been adopted from ref⁴⁴.

The RI-CC2 calculations show that the vertical transition energies of the S₁-S₀ and S₂-S₀ of isoindole locate around 4.15 and 4.21 eV respectively. At the same level of theory, the adiabatic S₁-S₀ transition of isoindole has been determined to be 3.91 eV. Considering a +0.2 eV overestimation error of CC2 method, the corrected adiabatic-transition energy of isoindole (3.71 eV) is in the excellent agreement with its experimental band origin (3.70 eV), reported by Bonnett and Brown⁵³. Moreover, the S₁-S₀ transition energy of isoindole is at least 0.35 eV higher than corresponding transition energy of indole molecule.

Similar to indole, the S₂-S₀ electronic transition of isoindole, has a ¹πσ* character. The vertical transition energy of this state has been determined to be 4.21 eV and 4.84 eV respectively for

isoindole and indole. More information from geometry and electronic structure of isoindole can be found in ESI file.

We have determined the geometry and electronic properties of quinoline at MP2 and CC2/aug-cc-pVDZ level of theory. The optimized geometry of quinoline has been presented in Figure 1 and the xyz coordinates have been presented in ESI file. The structure is planar, containing a C_s symmetry plane. The CNC bond angle is 117.2° , the CCC angles in the pyridine ring are variable between 119° - 124° , while they are roughly constant around 120° in the adjacent benzene ring. The C-N bond lengths are 1.376 \AA and 1.335 \AA , the former is related to the C-N which is in neighbourhood of benzene ring and the later is related to the second C-N bond.

Regarding the electronic transitions on the basis of CC2 calculation results, the first $^1A'$ excited state of quinoline corresponds to the S_1 - S_0 electronic transition, and the first $^1A''$ state corresponds to the second (S_2 - S_0) electronic transition. All of 10 singlet electronic transitions are in the UV range (4.37-6.31eV). The S_1 - S_0 , S_3 - S_0 and S_6 - S_0 , have large oscillator strength (0.025-0.63), while the rest transitions are approximately dark (i.e. having small oscillator strength; 0.000-0.001).

The frontier molecular orbitals (MOs) of the quinoline monomer are shown in Figure 3. From the RI-CC2 calculations, the S_1 ($1-^1A'$) state, corresponds to the orbital transition from HOMO-1 to LUMO+5 (58%) and HOMO-LUMO+9 (29%). It is obvious that the HOMO has a π character and LUMO+5, LUMO+9, both are of the π^* nature (from Fig.3), thus the S_1 state of quinoline has the $^1\pi\pi^*$ feature. In addition, the S_2 ($1-^1A''$) state of the quinoline corresponds to the orbital transition from HOMO-3 to LUMO+5 (90%), in which the HOMO-3 is of the nonbonding character (n) and LUMO+5 is of the π^* nature, thus the S_2 state is mostly of the $^1n\pi^*$ character.

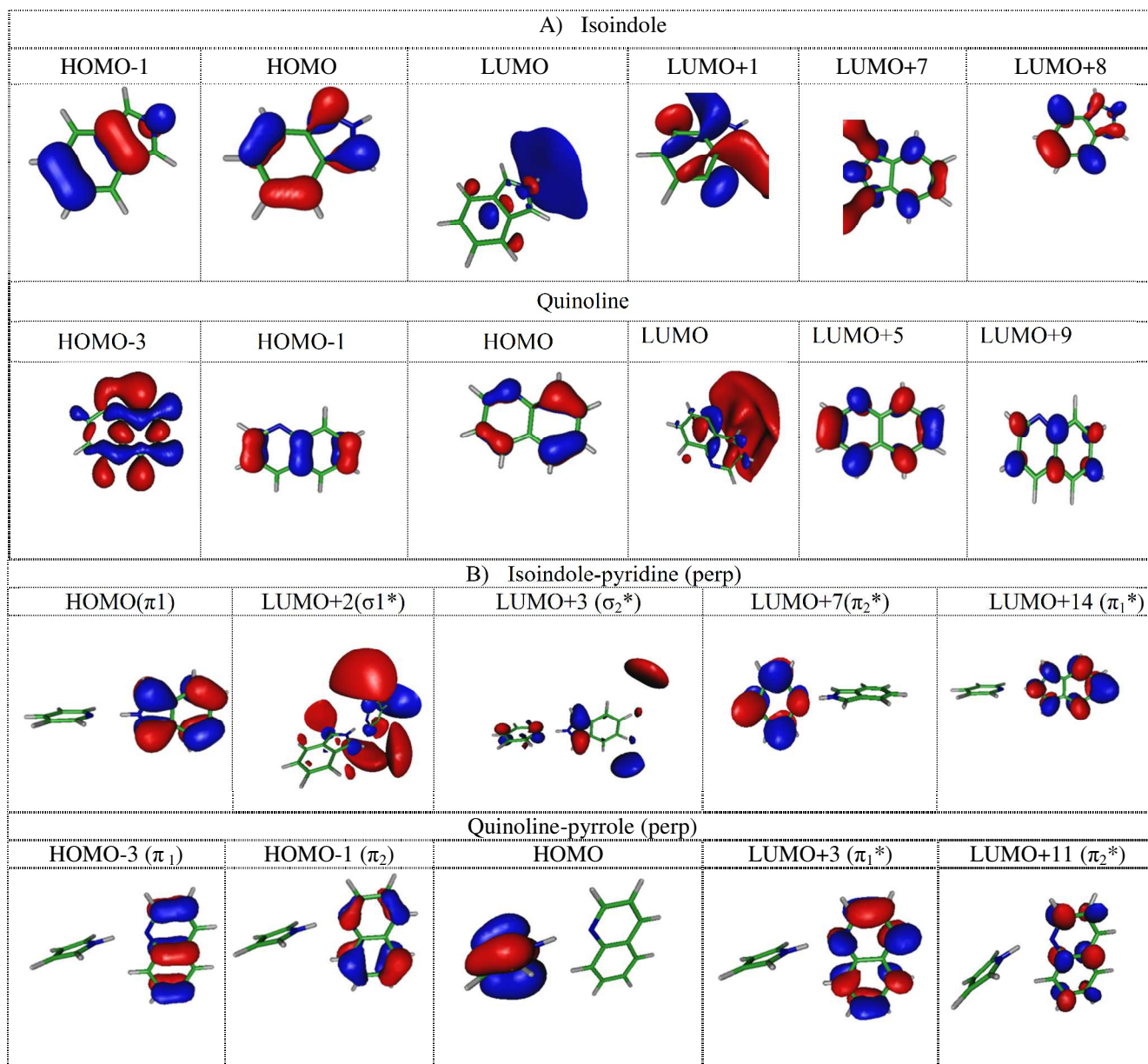


Figure 3. Selected frontier molecular orbitals of; A) isoindole and quinoline monomers and B) isoindole-pyridine, quinoline-pyrrole complexes.

3.2. Ground state equilibrium structures and excitation energies of complexes:

We have considered two types of complexes, isoindole-pyridine (*iIn-Pn*), and quinoline-pyrrole (*Q-Pl*). Each complex, has been constructed from a photo-acid (i.e. a proton donor) and a photo-

base (i.e. a proton acceptor moiety)²⁶. The photo-acid and photo-base systems have been connected by a strong hydrogen bond. In addition to regular hydrogen bond complexes, it is possible that these type monomers form stack structures, interacting in approximately parallel arrangement of monomers. Nevertheless, we have found that stack structures are at least 0.30 eV ($\sim 30 \text{ kJ.mol}^{-1}$) less stable than those of regular hydrogen bonded systems. In addition, the H-bonded complexes are more abundant in biological systems than stack structures. Thus we have disregarded to consider stack structures in present work.

We have considered three hydrogen-bonded configurations for each complex. All of the conformers have been optimized based on the MP2/aug-cc-pVDZ level of calculation. The optimized structures have been presented in Figure 2. As shown, in addition to two symmetric configuration for each complex; (perpendicular and planar), there is a full optimized configuration, for which no symmetry constraint has been applied during the S_0 optimization. For the case of *iIn-Pn*, the minimum unconstrained geometry (Fig. 2-c) is almost identical to perpendicular conformer (Fig. 2-a), with the same energy stability. The perpendicular and planar structures belong to the C_{2v} and C_s symmetry point groups respectively. The planar structure is 0.03 eV less stable than perpendicular one.

For quinoline-pyrrole (*Q-Pl*), both perpendicular and planar structures belong to the C_s symmetry point group. Similar to the case of *iIn-Pn* complex, the minimum unconstrained geometry of *Q-Pl* (Fig. 2-f) is almost the same as that of the perpendicular conformer (Fig. 2-d), which are 0.06 eV (5.79 kJ.mol^{-1}) more stable than planar. Thus, the perpendicular conformer will be representative for the unconstrained geometry of both complexes. In all conformers, there is a strong hydrogen bond between the N-H \cdots N moieties. The geometric parameters of hydrogen bond in the planar and perpendicular conformers of *iIn-Pn* are approximately identical, the N \cdots H hydrogen bond in perpendicular and planar are 1.870 Å and 1.889 Å respectively, indicating to slightly strengthening of hydrogen-bond in perpendicular structure. For the case of *Q-Pl* complex, the H \cdots N, N-H bond lengths and N-H-N bond angle in planar forms are 1.932 Å, 1.03 Å and 177° respectively and they are 1.849 Å, 1.029 Å and 160.2° for perpendicular form. This comparison also is consistent with strengthening of hydrogen bond in perpendicular conformer. The binding energies of the intermolecular hydrogen H \cdots N bond in the perpendicular and planar conformers of *iIn-Pn* are -0.48 eV and -0.45 eV, respectively, at the RI-MP2 level (the same difference in stability is found when the ZPE is taken into account). The binding energy has been

estimated for the two conformers of *Q-Pl* (perpendicular and planar) to -0.49 eV and -0.43 eV respectively.

The vertical transition energies of all considered conformers have been calculated on the optimized geometry of ground state. In *iIn-Pn* (perpendicular conformer, C_{2v}), the first 1B_2 excited state corresponds to the S_1-S_0 , and the first 1A_2 state corresponds to the second (S_2-S_0) electronic transitions. The S_1 and S_2 electronic transitions have been determined to be 4.04 and 4.17 eV respectively. The frontier molecular orbitals (MOs) of the *iIn-Pn* complex are shown in Figure. 3. From the RI-CC2 calculations, the S_1 (1B_2) state, has the largest oscillator strength among the lowest six electronic transition of *iIn-Pn* complex, corresponding mostly to the single electron transition from HOMO to LUMO+14 (73%). From Figure 3, it is seen that HOMO is a π orbital and LUMO+14 has π^* character, so the S_1 state of *iIn-Pn* complex is of the $^1\pi\pi^*$ feature. Because both of the HOMO and LUMO+14 localize on the isoindole moiety, the S_1 ($^1\pi\pi^*$) state is quite local transition. In addition, the S_2 (1A_2) state of this complex corresponds to the orbital transition from HOMO to LUMO+2 (47%) and HOMO to LUMO (18%), in which the HOMO π orbital, locates over the isoindole, and the LUMO+2 and LUMO, locate over the pyridine moiety, having σ^* nature. Thus the S_2 state has a CT- $^1\pi\sigma^*$ character.

Moreover, the first 1B_1 excited state of the *iIn-Pn*, corresponds to the S_3-S_0 electronic transition, which is mostly arising from HOMO-LUMO+7 single electron transition. From inspection of Figure 3, it is seen that the S_3-S_0 electronic transition of *iIn-Pn* has charge transfer (CT)- $^1\pi\pi^*$ nature. The HOMO π orbital locates over isoindole and LUMO+7, having π^* nature, locates over pyridine moiety.

In *Q-Pl*, the (perpendicular conformer), the first two excited states (S_1 , S_2) belong to the A' representation, while the first $^1A''$ state corresponds to the third (S_3-S_0) electronic transition.

	Electronic state	Vertical Transition Energy/eV	Oscillator strength	Adiabatic Transition Energy/eV
iIn-Pn, perp	S ₁ (B ₂) [LE- $\pi\pi^*$]	4.04	0.0668	3.79
	S ₂ (A ₂) [CT- $\pi\sigma^*$]	4.17	0.0000	-
	S ₃ (B ₁) [CT- $\pi\pi^*$]	4.29	0.0000	-
iIn-Pn, planar	S ₁ (B ₁) [LE- $\pi\pi^*$]	4.04	0.0627	3.79
	S ₂ (A ₂) [CT- $\pi\sigma^*$]	4.18	0.0000	-
	S ₃ (B ₁) [CT- $\pi\pi^*$]	4.33	0.0017	-
Q-PI, perp.	S ₁ (A') [LE- $\pi\pi^*$]	4.35	0.0260	4.20
	S ₂ (A') [CT- $\pi\pi^*$]	4.49	0.0268	-
	S ₅ (A'') [CT- $\pi\sigma^*$]	5.08	0.0000	-
Q-PI, planar	S ₁ (A') [LE- $\pi\pi^*$]	4.36	0.0257	4.21
	S ₂ (A') [CT- $\pi\pi^*$]	4.47	0.0025	-
	S ₅ (A'') [CT- $\pi\sigma^*$]	5.01	0.0002	-

Table 2: Excited transition energies (vertical and adiabatic), of isoindole-pyridine and quinoline-pyrrole complexes, computed at the CC2/aug-cc-pVDZ level of theory. The CC2 geometry optimization at the S₂ and S₃ excited states is accompanied with the large deformations, thus, we were unable to report their corresponding adiabatic transition energies.

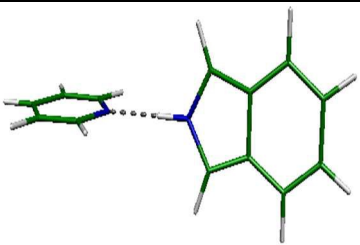
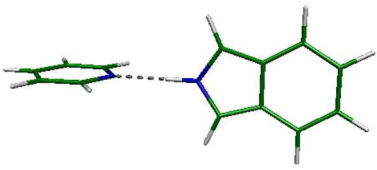
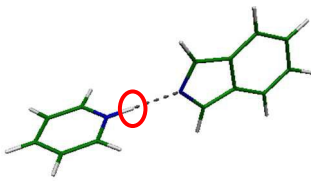
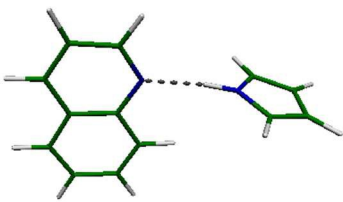
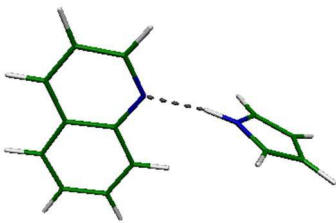
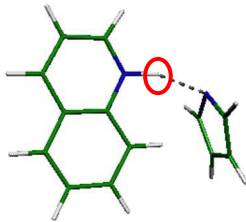
Isoindole-Pyridine		
a) Ground state (S_0)	b) S_1 [$LE-\pi\pi^*$]	c) S_3 [$CT-\pi\pi^*$]
 <p>a; 1.870 b; 1.035 θ; 180.0</p> <p>a; N...H b; H-N</p>	 <p>a; 1.783 b; 1.046 θ; 180.0</p>	 <p>a; 1.027 b; 1.988 θ; 180.0</p>
Quinoline – Pyrrole		
d) Ground state (S_0)	e) S_1 [A'_1 , $LE-\pi\pi^*$]	f) S_2 [$CT-\pi\pi^*$]
 <p>a; 1.030 b; 1.941 θ; 172.2</p>	 <p>a; 1.033 b; 1.921 θ; 170.2</p>	 <p>a; 1.900 b; 1.116 θ; 160.0</p>

Figure 4. Comparison between the optimized structures of *iIn-Pn* and *Q-Pl* complexes at the ground and $LE-\pi\pi^*$, $CT-\pi\pi^*$ excited states. The red circles indicate the transferred proton.

From the RI-CC2 calculations, the S_1 ($^1A'$) state, has a large oscillator strength, corresponding to the orbital transition from HOMO-3 to LUMO+3 (54%) and HOMO-1 to LUMO+11 (22%). From Figure 3, it is seen that the HOMO-1 and HOMO-3 have π character and LUMO+3 and LUMO+11 have π^* nature, thus the S_1 state of *Q-Pl* complex can be assigned as the $^1\pi\pi^*$ nature. Because all of the MOs, having important contributions in the S_1-S_0 transition of *Q-Pl* complex, localized over quinoline moiety, the S_1 ($^1\pi\pi^*$) state is quite local transition. In addition, the S_2 ($^1A'2$) state of this complex mostly corresponds to the orbital transition from HOMO to LUMO+3, in which the HOMO, π orbital, locates over the pyrrole monomer, and the LUMO+3,

π^* orbital, locates over the quinoline moiety. Thus the S_2 state, is a ${}^1\pi\pi^*$ state, having significantly CT character.

3.3. Excited-state minimum geometries and adiabatic excitation energies

The excited-state optimized geometries are required for determination of adiabatic electronic transition energies, which are more appropriate for comparing with corresponding experimental 0-0 bands. In addition, the optimized geometry of excited state can be a good sign for photophysical exploration, based on the large geometry deformations, hydrogen/proton transfer⁵⁶ processes and ring opening/ ring puckering alterations^{57, 58}. There is a large possibility for each type of deformations to be responsible for an ultrafast non-radiative relaxation pathway of excited systems to the ground via conical intersections⁴⁶. Thus we have determined the local and CT- ${}^1\pi\pi^*$ optimized geometry of each complex at the RI-CC2/aug-cc-pVDZ level of theory. The results relevant to the most stable conformers will be briefly discussed.

For isoindole-pyridine complex, the most stable conformer is a perpendicular structure, belongs to the C_{2v} symmetry point group. We have optimized the S_1 (1B_2), S_2 (1A_2) and S_3 (1B_1) states of this conformer, at the RI-CC2/aug-cc-pVDZ level of theory. In Fig. 4, a comparison of minimum structures between the ground and excited states of the perpendicular conformer has been presented. For this conformer, the lowest excited singlet state is of LE- ${}^1\pi\pi^*$ character. Following photoexcitation of this conformer, the $H\cdots N$ hydrogen bond decreases by 0.087 Å, while the N–H distance increases by 0.011 Å (Fig. 4-a and b). As a consequence, the binding energy of the intermolecular hydrogen bond $H\cdots N$ between isoindole and pyridine greatly increases from -0.48 eV to -0.60 eV, which shows slightly increasing after excitation. However, the second electronic transition of isoindole-pyridine, is of the ${}^1\pi\sigma^*$ character; the π orbital localized on isoindole part and the σ^* orbital mostly locate over the pyridine moiety. Thus the ${}^1\pi\sigma^*$ state has CT character. The minimum geometry of *iIn-Pn* (for both conformers), has been determined based on the CC2 geometry optimization. The excited state proton transfer takes place from isoindole to pyridine moiety.

Moreover, the third electronic transition of isoindole-pyridine (S_3 - S_0), is of the charge transfer ${}^1\pi\pi^*$ character, (i.e. from isoindole to pyridine). The minimum geometry of *iIn-Pn*, has been determined based on the CC2 geometry optimization (Figure 4-c). As shown, at the excited S_3 state, the N-H proton of isoindole transfers to the pyridine's N atom. The N-H distance in

pyridine part has been determined to 1.074 Å, and the H...N, is 1.687 Å. Also, for the planar conformer of isoindole-pyridine, the lowest three electronic transitions have the same characters as perpendicular complex.

The optimized geometry of the two first excited states of quinoline-pyrrole, for its most stable conformer (perpendicular), can be compared with its ground state structure from Figure 4 (d-e). The optimized ground state structure belongs to the C_s symmetry point group. The first and second electronic transitions are LE- $^1\pi\pi^*$ and CT- $^1\pi\pi^*$ states respectively. The minimum geometry (Fig. 4-b) of the lowest excited singlet state; S_1 (LE- $^1\pi\pi^*$), does not show significant geometry alteration. Nevertheless the S_2 (CT- $^1\pi\pi^*$) geometry optimization has been predicted to be accompanied with proton transfer from pyrrole to quinoline moiety.

The adiabatic excitation energies and corresponding oscillator strengths of the two lowest excited singlet states of the two considered conformers of *iIn-Pn* and *Q-Pl* complexes optimized by RICC2/aug-cc-pVDZ calculation have been presented in Table 2. The adiabatic transition energy of the S_1 ($^1\pi\pi^*$)- S_0 for the most stable conformers of isoindole-pyridine and quinoline-pyrrole have been determined to 3.79 eV and 4.21 eV respectively.

Unfortunately, there is no experimental value relevant to electronic transitions of titled dimmers to be considered for evaluation of our theoretical results. However, in previous sections for the S_1 - S_0 determination of individual monomers, we have clarified that our theoretical level of calculations shows approximately 0.20 eV overestimation error^{59, 52}. Thus the corrected adiabatic transition energy of *iIn-Pn* and *Q-Pl* will be amount to 3.59 eV and 4.01 eV respectively.

3-4. Potential energy profiles and internal conversions:

3-4-1. Isoindole-pyridine:

The CC2 geometry optimization of isoindole-pyridine complex at the S_3 (1B_1 - $^1\pi\pi^*$) state leads to proton transfer from isoindole chromophore to pyridine. Thus we have been motivated to investigate the PE profiles of this complex along the PT reaction coordinate. In Figure 5, the CC2 PE profiles calculated along the minimum-energy path for proton transfer from the isoindole N-H group to the N atom of pyridine are presented. For clarity, only the lowest three excited singlet states (LE- $^1\pi\pi^*$, CT- $^1\pi\sigma^*$ and CT- $^1\pi\pi^*$ states) along with the electronic ground state are displayed. The geometries of all solid curves have been optimized along the reaction

path, while the dash line (i.e. ground-state PE profile) is computed at the CT- $^1\pi\pi^*$ optimized geometries as a complementary potential energy curve. Thus, the S_1^{S1} denotes the energy of the S_1 state calculated along the reaction path, optimized in the S_1 state (without symmetry constraint), while the $S_1^{S1}(\pi\pi^*\text{-LE})$ denotes the energy of the S_1 state calculated along the reaction path optimized in the $S_1(\pi\pi^*\text{-LE})$ state, under the C_s symmetry constraint. Also, the S_0^{S0} notation denotes the energy of the S_0 state calculated along the reaction path optimized in the S_0 state, etc.

From inspection of results presented in Figure 5, it is seen that the PE profiles of the ground state, and the lowest valence LE- $^1\pi\pi^*$ excited states increase with increasing N-H distance, while the PE profile of the CT- $^1\pi\pi^*$ state is essentially repulsive. The increasing trend of S_0 PE profile indicates that ground state hydrogen/proton transfer process in isoindole-pyridine is extremely unlikely since of its endoenergetic nature ($\Delta E > 1.0$ eV). The repulsive CT- $^1\pi\pi^*$ PE profile crosses with the LE- $^1\pi\pi^*$ and the CT- $^1\pi\sigma^*$ MPE profiles at the beginning of reaction coordinate, and then intersects with the S_0 potential energy profile at the end of reaction path, where the proton is entirely transferred to pyridine moiety. In a multidimensional picture, the CT-($^1\pi\pi^*$)- S_0 curve crossing in Figure 5 develops into a conical intersection (CI)^{16, 17, 19, 60}. Although there are two CIs (LE- $^1\pi\pi^*$ /CT- $^1\pi\sigma^*$ and CT- $^1\pi\pi^*$ /LE- $^1\pi\pi^*$) at the beginning of reaction coordinate, the latest CI (CT- $^1\pi\pi^*$ - S_0) is real, because its relevant PE profiles (i.e. CT- $^1\pi\pi^*$ and the S_0 state) have been determined based on the same optimized geometries. This conical intersection can be responsible for ultrafast nonradiative relaxation of isoindole-pyridine complex, after photoexcitation to the S_1 LE-($^1\pi\pi^*$) excited state.

One may be concerned from the barrier existing on the beginning of reaction coordinate, in the region where LE-($^1\pi\pi^*$) intersects with CT-($^1\pi\pi^*$) excited state. We have determined the adiabatic PE profile of the coupled LE-($^1\pi\pi^*$)-CT-($^1\pi\pi^*$). This PE sheet has been determined based on the S_1 geometry optimization, without any symmetry constraint. In this manner, the vibronic coupling between the LE- $^1\pi\pi^*$ and CT- $^1\pi\pi^*$ will be allowed. However, the adiabatic PE profile exhibits no barrier in the vicinity of the conical intersection. The barrier-less S_1 potential energy curve, indicates to an ultrafast dynamics of ESHT/PT process from isoindole to pyridine moiety.

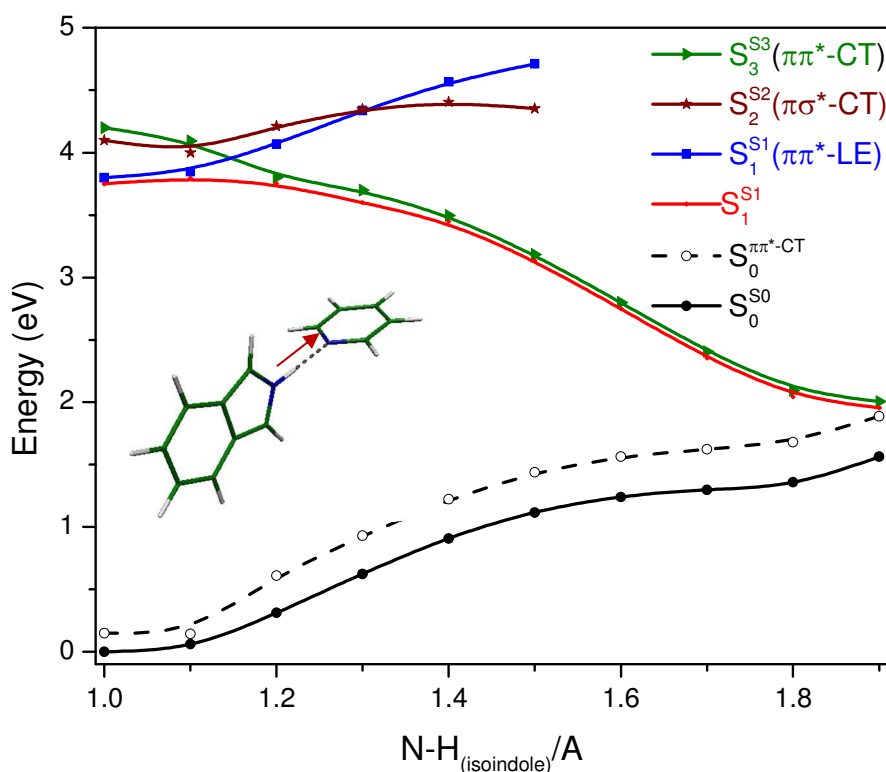


Figure 5: CC2 PE profiles of isoindole-pyridine complex at the electronic ground state and few excited states, as a function of the N-H stretching coordinate. Full lines represent the minimum energy profiles of reaction paths determined in the same electronic state ($S_0^{(S_0)}$, $S_1^{(S_1)}$, ...), while the dashed line ($S_0^{(\pi\pi^*)}$), stands for the energy profile of ground state determined based on the optimized complementary electronic S_3 (CT- $\pi\pi^*$) state. The red coloured curve, shows the minimum S_1 potential energy profile of the isoindole-pyridine determined based on the CC2 geometry optimization of S_1 state without symmetry considerations.

Furthermore, the credibility of the RI-CC2, as a single reference method, for determination of excited state potential energy profiles, is a subject of question. However, this matter has been investigated previously⁵¹ by comparison the CC2 PE results with accurate CASPT2 and MR-AQCC data. It has been established that RI-CC2 predicts qualitatively reliable energy profiles and, its results are reliable for the qualitative determination of PE profiles^{2, 15, 61-64}.

3-4-2. Quinoline-Pyrrole

In Figure 6, the CC2 PE profiles calculated along the minimum-energy path for proton transfer between pyrrole and quinoline have been presented. Only the lowest LE- ${}^1\pi\pi^*$, CT- ${}^1\pi\pi^*$ and the electronic ground state are displayed. However, for determination of potential energy curves, the geometries of the ground and excited states have been optimized along the reaction path, while a complementary ground state PE profile has been determined on the basis of the CT- ${}^1\pi\pi^*$ optimized geometries. The reaction coordinate is defined as the N-H bond distance of pyrrole monomer and describes the position of the proton relative to the nitrogen atom of pyrrole. It is seen that the PE profiles of the ground state and the lowest ${}^1\pi\pi^*$ excited state slightly increase with increasing the reaction coordinate, while the CT- ${}^1\pi\pi^*$ profile has decreasing pattern.

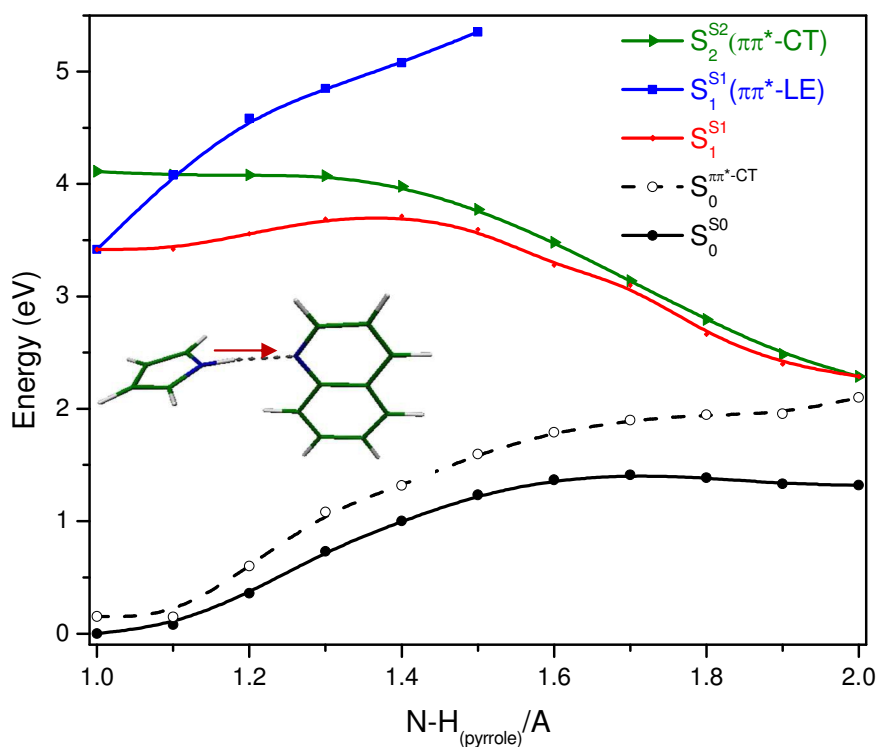


Figure 6: CC2 PE profiles of quinoline-pyrrole complex at the electronic ground state and few excited states, as a function of the N-H stretching coordinate.

From increasing trend of S_0 PE profile of Figure 6, it is seen that the ground state hydrogen/proton transfer (GSHT/PT) process from pyrrole to quinoline is quite unlikely since of its endoenergetic nature; (needing at least 1.0 eV energy). Nevertheless, the minimum potential energy curve of the $CT-^1\pi\pi^*$ state shows a decreasing trend following a flat structure at the beginning of reaction coordinate. Thus, it crosses with the local $^1\pi\pi^*$ PE profile and latter, at the end of reaction coordinate, it approaches to the ground state PE sheet. Although our results do not show exactly the curve crossing between $CT-^1\pi\pi^*$ state of quinoline-pyrrole complex with that of the S_0 state, at the end of reaction coordinate, the difference between these two levels is only 0.10 eV. This small energetic-gap, significantly increases the electronic-coupling possibilities between two states, which can play the role of a curve crossing at the end of reaction coordinate.

It is noteworthy that the RI-CC2 method, owing to its single reference nature, is not appropriate for treatment of regions which have strong multi-reference characters such as conical intersections and bond breaking regions. Instead, that is trustworthy for the qualitative determination of PE profiles in these regions⁶¹⁻⁶⁵.

The resulting lower adiabatic PE sheet of the coupled $LE-^1\pi\pi^*/CT-^1\pi\pi^*$ states exhibits a small barrier roughly in the middle of reaction coordinate, corresponding to the position where proton locates between two monomers. We have evaluated this barrier by breaking the C_s symmetry of the system. The barrier has been estimated amount to 0.30 eV. In the gas phase, a wave packet prepared in the $LE-^1\pi\pi^*$ state of quinoline-pyrrole complex, by optical excitation with sufficient excess energy (≈ 0.3 eV) will bypass this barrier and then evolve on the $CT-^1\pi\pi^*$ surface. The low-energy part of the $^1\pi\pi^*$ surface is separated from the region of strong non-adiabatic interactions with the ground state by this barrier on the PE surface of the lowest excited singlet state.

4- Conclusion

Ab initio electronic-structure and reaction-path calculations have been performed to characterize the intra-cluster proton-transfer processes in isoindole-pyridine and quinoline-pyrrole complexes. It has been predicted that nonradiative deactivation mechanism in the titled

complexes, is mostly governed by the N–H bond stretching and the S_1/S_0 conical intersections. The PE profile of the CT- $^1\pi\pi^*$ state is dissociative along the N–H reaction path. The N–H bond elongation, mediated by coupled electron/proton transfer, leads to deactivation via CT- $^1\pi\pi^*/S_0$ conical intersection. In this respect, two readily accessible conical intersections of LE- $\pi\pi^*/CT-^1\pi\pi^*$ and CT- $^1\pi\pi^*/S_0$ in the gas phase, which are encountered along the reaction path, are responsible for nonradiative relaxation of these type complexes. However, for the isoindole-pyridine complex, this relaxation pathway has been predicted to be quite barrier-free, while in the quinoline-pyrrole case, a barrier of 0.30 eV in the middle of reaction coordinate, prohibits the excited wave-packet from FC region of LE- $^1\pi\pi^*$ to proceed quickly along the N–H reaction coordinate. Nevertheless, the tunneling effect of hydrogen atom through this barrier increases the possibility of its access to the dissociative part of the S_1 PE profile. The conical intersection arisen from coupled electron/proton transfer process in quinoline-pyrrole complex can be responsible for ultrafast nonradiative deactivation of the S_1 excited system to the ground via internal conversions.

Acknowledgment

The research council of *Isfahan University* is acknowledged for financial support. We kindly appreciate the use of computing facility cluster GMPCS of the LUMAT federation (FR LUMAT2764).

References:

1. G.-J. Zhao and K.-L. Han, *Accounts. Chem. Res.*, 2011, **45**, 404-413.
2. A. L. Sobolewski and W. Domcke, *J. Phys. Chem. A.* , 2007, **111**, 11725-11735.
3. S. Olsen and S. C. Smith, *J. Am. Chem. Soc.* , 2008, **130**, 8677-8689.
4. C.-H. Tung, L.-Z. Wu, L.-P. Zhang and B. Chen, *Accounts. Chem. Res.* , 2003, **36**, 39-47.
5. D. Jacquemin, J. Zúñiga, A. Requena and J. P. Céron-Carrasco, *Acc. Chem. Res.*, 2014, **47**, 2467-2474.
6. H. Wang, J. D. Zhang and H. F. Schaefer, *ChemPhysChem*, 2010, **11**, 622-629.
7. J. D. Watson and F. H. C. Crick, *Nature*, 1953, **171**, 964-967.
8. J. DeChancie and K. Houk, *J. Am. Chem. Soc.* , 2007, **129**, 5419-5429.

9. F. M. Raymo, M. D. Bartberger, K. Houk and J. F. Stoddart, *J. Am. Chem. Soc.* , 2001, **123**, 9264-9267.
10. Q. Sun, M. Doerr, Z. Li, S. C. Smith and W. Thiel, *Phys. Chem. Chem. Phys.* , 2010, **12**, 2450-2458.
11. R. Daengngern, N. Kungwan, P. Wolschann, A. J. A. Aquino, H. Lischka and M. Barbatti, *J. Phys. Chem. A*, 2011, **115**, 14129-14136.
12. G. Féraud, M. Berdakin, C. Dedonder, C. Jouvét and G. A. Pino, *J. Phys. Chem. B*, 2015, **119**, 2219-2228.
13. T. Shimizu, S. Manita, S. Yoshikawa, K. Hashimoto, M. Miyazaki and M. Fujii, *Phys. Chem. Chem. Phys.*, 2015.
14. M. F. Rode and A. L. Sobolewski, *Chem. Phys.*, 2008, **347**, 413-421.
15. A. L. Sobolewski, W. Domcke and C. Hättig, *Proc. Nat. Acad. Sci. US.*, 2005, **102**, 17903-17906.
16. D. R. Yarkony, *J. Phys. Chem. A*, 2001, **105**, 6277-6293.
17. S. Matsika and P. Krause, *Ann. Rev. Phys. Chem.*, 2011, **62**, 621-643.
18. D. R. Yarkony, *Acc. Chem. Res.*, 1998, **31**, 511-518.
19. J. D. Coe and T. J. Martínez, *J. Am. Chem. Soc.*, 2005, **127**, 4560-4561.
20. M. Esboui and N. Jaidane, *Photochem. Photobiol. Sci.*, 2015, **14**, 1127-1137.
21. C. Randino, M. Ziółek, R. Gelabert, J. A. Organero, M. Gil, M. Moreno, J. M. Lluch and A. Douhal, *Phys. Chem. Chem. Phys.* , 2011, **13**, 14960-14972.
22. A. L. Sobolewski and W. Domcke, *Phys. Chem. Chem. Phys.* , 1999, **1**, 3065-3072.
23. A. L. Sobolewski and W. Domcke, *Phys. Chem. Chem. Phys.* , 2006, **8**, 3410-3417.
24. S. Scheiner, *J. Phys. Chem. A*, 2000, **104**, 5898-5909.
25. A. L. Sobolewski and W. Domcke, *J. Phys. Chem. A* , 2001, **105**, 9275-9283.
26. L. M. Frutos, A. Markmann, A. L. Sobolewski and W. Domcke, *J. Phys. Chem. B* , 2007, **111**, 6110-6112.
27. T. L. Gilchrist, *Heterocyclic Chemistry (3rd Edition)*, 1997, **Oxford Primer Series**.
28. V. Dryza, J. A. Sanelli, E. G. Robertson and E. J. Bieske, *J. Phys. Chem. A* , 2012, **116**, 4323-4329.
29. J. Bouwman, B. Sztaray, J. Oomens, P. Hemberger and A. Bodi, *J. Phys. Chem. A* , 2015, **119**, 1127-1136.
30. R. Ahlrichs, M. Bär, M. Häser, H. Horn and C. Kölmel, *Chem. Phys. Lett.* , 1989, **162**, 165-169.
31. TURBOMOLE, V6.3 2011, a development of University of Karlsruhe and Forschungszentrum Karlsruhe GmbH, 1989-2007, TURBOMOLE GmbH, since 2007; available from <http://www.turbomole.com>.
32. F. Weigend and M. Häser, *Theor. Chem. Acc.*, 1997, **97**, 331-340.
33. F. Weigend, M. Häser, H. Patzelt and R. Ahlrichs, *Chem. Phys. Lett.* , 1998, **294**, 143-152.
34. O. Christiansen, H. Koch and P. Jørgensen, *Chem. Phys. Lett.* , 1995, **243**, 409-418.
35. C. Hättig, *J. Chem. Phys.*, 2003, **118**, 7751-7761.
36. T. H. Dunning Jr, *J. Chem. Phys.* , 1989, **90**, 1007-1023.
37. M. Becucci, N. M. Lakin, G. Pietraperzia, P. R. Salvi, E. Castellucci and E. R. T. Kerstel, *J. Chem. Phys.* , 1997, **107**, 10399-10405.
38. Z.-L. Cai and J. R. Reimers, *J. Phys. Chem. A*, 2000, **104**, 8389-8408.
39. R. M. Hochstrasser and J. W. Michaluk, *J. Chem. Phys.*, 1971, **55**, 4668-4669.
40. M. Barbatti, M. Vazdar, A. J. Aquino, M. Eckert-Maksić and H. Lischka, *J. Chem. Phys.*, 2006, **125**, 164323.
41. O. Christiansen, J. Gauss, J. F. Stanton and P. Jørgensen, *J. Chem. Phys.*, 1999, **111**, 525-537.
42. B. Cronin, A. L. Devine, M. G. D. Nix and M. N. R. Ashfold, *Phys. Chem. Chem. Phys.*, 2006, **8**, 3440-3445.

43. M. Chachisvilis and A. H. Zewail, *J. Phys. Chem. A.*, 1999, **103**, 7408-7418.
44. K. K. Innes, I. G. Ross and W. R. Moomaw, *J. Mol. Spect.*, 1988, **132**, 492-544.
45. M. Szafran and J. Koput, *J. Mol. Struct.*, 2001, **565-566**, 439-448.
46. A. L. Sobolewski and W. Domcke, *Chem. Phys.*, 2000, **259**, 181-191.
47. A. L. Sobolewski and W. Domcke, *Chem. Phys. Lett.*, 1999, **315**, 293-298.
48. K. Somers, E. Kryachko and A. Ceulemans, *Chem. Phys.*, 2004, **301**, 61-79.
49. A. Mani and J. R. Lombardi, *J. Mol. Spect.*, 1969, **31**, 308-317.
50. R. Bersohn, U. Even and J. Jortner, *J. Chem. Phys.*, 1984, **80**, 1050-1058.
51. A. J. A. Aquino, H. Lischka and C. Hättig, *J. Phys. Chem. A.*, 2005, **109**, 3201-3208.
52. I. Alata, C. Dedonder, M. Broquier, E. Marceca and C. Jouvet, *J. Am. Chem. Soc.*, 2010, **132**, 17483-17489.
53. R. Bonnett and R. F. C. Brown, *J. Chem. Soc. Chem. Comm.*, 1972, 393-395.
54. I. Yamazaki and H. Baba, *J. Chem. Phys.*, 1977, **66**, 5826-5827.
55. M. Bavia, F. Bertinelli, a. C. Taliani and C. Zauli, *Mol. Phys.*, 1985, **31**, 479.
56. M. Ataelahi, R. Omidyan and G. Azimi, *Photochem. Photobiol. Sci.*, 2015, **14**, 457-464.
57. R. Omidyan and H. Rezaei, *Phys. Chem. Chem. Phys.*, 2014, **16**, 11679-11689.
58. B. Saed and R. Omidyan, *J. Phys. Chem. A.*, 2013, **117**, 2499-2507.
59. A. J. A. Aquino, F. Plasser, M. Barbatti and H. Lischka, *Croat. Chem. Acta.*, 2009, **82**, 105-113.
60. D. R. Yarkony, *Acc. Chem. Res.*, 1998, **31**, 511-518.
61. A. L. Sobolewski and W. Domcke, *Phys. Chem. Chem. Phys.*, 2006, **8**, 3410-3417.
62. A. L. Sobolewski and W. Domcke, *Chem. Phys. Chem.*, 2007, **8**, 756-762.
63. A. L. Sobolewski, W. Domcke and C. Hättig, *J. Phys. Chem. A.*, 2006, **110**, 6301-6306.
64. A. L. Sobolewski, D. Shemesh and W. Domcke, *J. Phys. Chem. A.*, 2008, **113**, 542-550.
65. M. F. Rode, A. L. Sobolewski, C. Dedonder, C. Jouvet and O. Dopfer, *J. Phys. Chem. A.*, 2009, **113**, 5865-5873.